Cross-slot extensional flow birefringence observations of polymer melts using a multi-pass rheometer

K. D. Coventry and M. R. Mackley[a]

Department of Chemical Engineering, University of Cambridge, Cambridge CB2 3RA, United Kingdom

Synopsis

This paper reports initial experimental flow birefringence studies of cross-slot flow for a range of molten polyethylenes using a multipass rheometer (MPR). An MPR was modified to accommodate a cross-slot center section insert thereby enabling small quantities of molten polymer to be evaluated in a near two-dimensional pure shear extensional flow. The results show that it was possible to obtain precise processing data for cross-slot flow using 10 g quantities of polymer. Experimental observations on different polyethylenes showed that in all cases the flow commenced from a Newtonian situation where the optical birefringent fringes around the central stagnation point were essentially symmetric. As the flow developed, the fringe pattern became progressively more asymmetric about the exit symmetry plane and the extent of the viscoelasticity of the polymer could be quantified by the observed level of anisotropy between the birefringence fringes on the entry and exit symmetry planes of the flow. The progressive development of anisotropy and stress with increasing extensional flow rate and type of polymer is presented for a number of flow conditions and it was found that increasing viscoelasticity of the polymer resulted in a progressive increase in viscoelastic center-line extensional stresses. The data provide benchmark large strain extensional flow experiments for certain polymer melts that can in the future be used to compare with numerical simulation. © *2008 The Society of Rheology.* [DOI: 10.1122/1.2836671]

I. INTRODUCTION

Large strain extensional flow deformations are capable of probing rheological aspects of polymer melt behavior that are not necessarily revealed in simple shear flow and as a consequence a range of rheometers have been designed for their study in extensional deformation. These rheometers can be broadly grouped into apparatus designed to stretch a sample and apparatus designed to generate flow around a stagnation point. The former group include rheometers such as the tensile extensional rheometer [see, for example, Meissner *et al.* (1981); Munstedt (1979)] and the filament stretching rheometer [Sridhar *et al.* (1991)]. More recently a simple tensile extension device has been developed to fit on a standard controlled shear strain rheometer [Sentmanat *et al.* (2005)]. Stagnation point flow was pioneered by G. I. Taylor for the extensional observation of droplet deformation in a four roll mill [Taylor (1934)]. An apparatus similar to Taylor's four roll mill was later used for the study of polymer solutions [see, for example, Crowley *et al.* (1976)]. The four roll mill generated useful results but was limited to relatively low

---

[a]Author to whom correspondence should be addressed; electronic mail: mrm5@cam.ac.uk

viscosity polymer solutions and suffered from problems with flow instabilities. To address some of these problems Scrivener *et al.* (1979) designed a cross-slot apparatus to generate a similar flow pattern, with two opposing flow channels with a central stagnation point and opposing orthogonal flow channels. The symmetry of this design provided well defined boundary conditions with a pure extensional flow in the central region near the stagnation point. A similar technique was later used by Miles and Keller (1980) for the study of polymer solution relaxation times.

A cross-slot device suitable for polymer melts was first developed by Verbeeten (2001), Verbeeten *et al.* (2002) and this required large quantities of polymers. This is also true of a recently built ETH polymer melt cross-slot device [Soulages *et al.* (2008)]. Odell *et al.* (2006) have recently developed a cross-slot oscillatory extensional flow device for probing the extensional dynamic behavior of polymer solutions and this device only requires small quantities for fluid, but at present the apparatus operates at room temperature. Pathak *et al.* (2006) also have also recently developed a low temperature micro-fluidic cross-slot apparatus for the study of micelle solutions.

In this paper a multipass rheometer (MPR) has been modified to generate highly controlled cross-slot flow with well defined boundary conditions. The MPR was originally designed as a two-piston capillary rheometer for use with small sample sizes [Mackley *et al.* (1995)], and subsequently it was modified to incorporate optical windows for flow birefringence studies [see, for example, Collis and Mackley (2005); Lee *et al.* (2001)]. In order to generate cross-slot flow, the basic action of the hydraulic pistons and barrels was retained and a new test section fabricated to accommodate cross-slot flow.

Cross-slot flow experiments are primarily suited to study through flow birefringence. The key element of the stagnation point flow is that as fluid elements progressively approach the stagnation point, they experience increasing levels of strain. To a first approximation the level of strain experienced by the fluid is inversely proportional to the distance from the exit symmetry plane and therefore in principle, fluid elements that pass through the stagnation point experience infinite strain [see, for example, Crowley *et al.* (1976)]. By examining flow birefringence stress fields it is therefore possible to explore a full range of strain histories for a given flow condition.

While it is possible to measure pressure difference using the MPR, the magnitude of pressure difference observed due to the extensional flow at the stagnation point is small when compared with the pressure drop in the inlet and outlet regions of the device. Thus it is difficult to measure the pressure drop that is directly related to localized extensional flow events in the central region of the cross-slot. The cross-slot MPR configuration is therefore best suited to flow birefringence studies where optical anisotropy profiles can be converted using a stress optical coefficient to create profiles of principal stress difference. Work by previous authors [see, for example, Venerus *et al.* (1999)] has shown that for stresses up to 1 MPa, the stress optical rule has not been violated. The maximum stresses reported in this paper are lower than 0.25 MPa, and so it assumed the stress optic coefficient (SOC) is valid for the polyethylenes studied in this particular geometry. It is not possible to directly measure the SOC in this apparatus because measurable pressure drops include significant contributions from the slit inlet and outlet flow. If future numerical simulations give a good quantitative match to experimental stress patterns then both the simulation and SOC will be validated.

For the purpose of optical birefringence it is easiest to approximate two-dimensional flow. The topic of the two-dimensional assumption has received some attention from other authors [see, for example, Wales (1976); Schoonen (1998); Clemeur *et al.* (2004); Soulages (2008)]. It has been shown by these authors that for depth to width ratios of greater than 8:1, the error in the retardation through the medium is of the order of 10%,
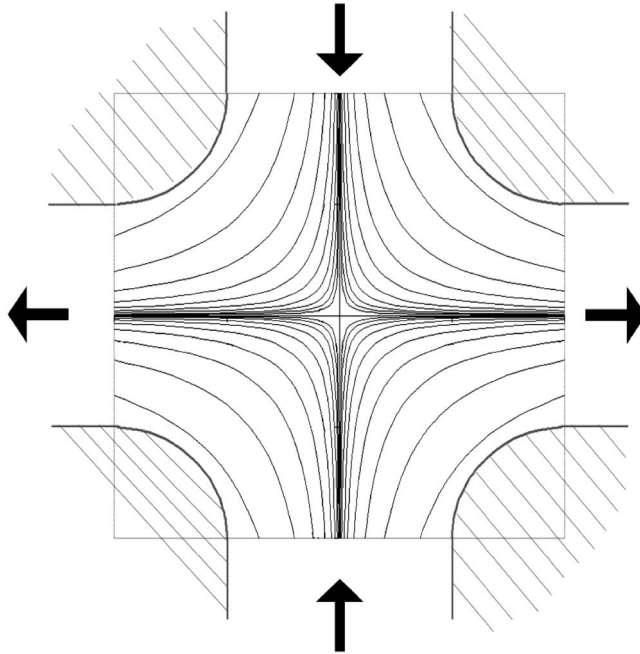
FIG. 1. Schematic diagram showing perfect flow with the test geometry superimposed.

and this has been supported by simulations carried out as part of this project [Coventry (2006)]. The velocity flow field has been shown by laser Doppler velocimetry (LDV) to be symmetric across both the horizontal and vertical axes with a point of zero velocity at the center. From the observed symmetry of the flow and given its two-dimensional nature, it can be inferred that the flow is a planar extensional flow along the symmetry axes.

The two-dimensional flow field observed from the birefringence experiments involves a range of different strain histories depending on location of the streamline—the closer a streamline passes to the stagnation point the higher the level of strain [Crowley *et al.* (1976)]. Thus for a chosen flowrate, a full range of strain histories can be observed in one picture. Using the two-dimensional assumption, the results of these experiments can be compared with the results of various numerical simulations.

This paper describes the modifications to the MPR to allow cross-slot flow and presents some preliminary findings. Birefringence images are presented as a function of time, central region extension rate and polymer architecture.

II. EXPERIMENTAL

A. Cross-slot flow in the MPR

Cross-slot flow involves two opposed inlet streams meeting at a planar stagnation point and then exiting orthogonally. The symmetry of the flow geometry is similar to the G.I. Taylor four-roll mill but in the case of the cross-slot, the boundary conditions are defined by stationary walls rather than moving rollers. Figure 1 shows the geometry of the cross-slot chosen for MPR experiments. Superimposed on the figure are the streamlines for a pure hyperbolic two-dimensional extensional flow and it can be envisaged that

near the central stagnation point the flows will match. Near the walls both the different contours and the no slip wall boundary condition will lead to a mixed flow.

The choice of cross-slot dimensions was dictated by a number of compromises relating to the apparatus, sample quantity under test, overall size and optic considerations. To ensure two-dimensional flow it would be desirable to have as large a channel depth to width ratio as possible, however the existing geometry of the MPR limited the test depth to a maximum of 10 mm. An inlet and outlet channel width of 1.5 mm was selected in order to enable clear optical resolution of fringes while maximizing the depth to width ratio. The dimensions of the cross-slot test section are shown in Fig. 2 and the cross-slot inserts that were manufactured based on this design are shown in Fig. 3. A very important aspect of the apparatus design is to ensure temperature control, and this was achieved by having the cross-slot inserts embedded within an internally heated center section.

The cross-slot action was achieved by driving the polymer melt into the central test section using the hydraulically driven MPR pistons. The fluid then flowed out of the side arms into small reservoirs in the test inserts. Slave pistons controlled by compressed air were fitted into the side inserts in order to contain the fluid in the test section so that multiple experiments could be carried out on the same sample. The servo hydraulic controlled pistons delivered a precise volumetric flowrate from which an approximate extension rate in the region of the stagnation point was calculated. From the geometry of the cross-slot, it can be deduced that the extension rate will be approximated by Eq. (1). The matching of some numerical simulations with experiment has shown this to be a reasonable representation of the central extension rate [see Coventry (2006)] and preliminary (LDV) experiments on the cross-slot flow also support this finding.

$$E = 2v_{avg}/w$$

E = Approximate central extension rate

v_{avg} = average fluid velocity in the inlet/outlet slit   (1)

w = width of the inlet slit

In the inlet regions, the flow approaches fully developed planar channel flow. At higher flow rates, there are some entrance effects that persist from the entrance region to the cross-slot, which is outside the field of view, but the results of these can be observed from the birefringence as a non-zero stress in the center of the channel. The magnitude of this persistent stress, however, is typically small compared with the extensional stress near the stagnation point. From observation of the transient images it is possible to determine exactly which fringe is the zero order fringe and thus account for the entrance effects. As the curvature in the walls develops in the region of the stagnation point, the flow changes to an approximation of hyperbolic flow and the fluid streamlines near the symmetry plane see progressively higher extensional strains. As the fluid then flows away from the stagnation point and into the exit slit, it reverts to planar channel flow, however, in the region of the exit symmetry plane, the viscoelastic memory of the extensional stresses can persist.

Optical birefringence images were obtained using a standard optical setup [see, for example, Fuller (1995)] consisting of a light source, monochromatic filter (514 nm with a width of light spectrum of 11.5 nm at half the maximum transmittance), polarizer and a quarter-wave plate before the sample to generate circularly polarized light, with a quarter-wave plate and an analyzer to resolve the image followed by a digital charge coupled device camera to capture the image.
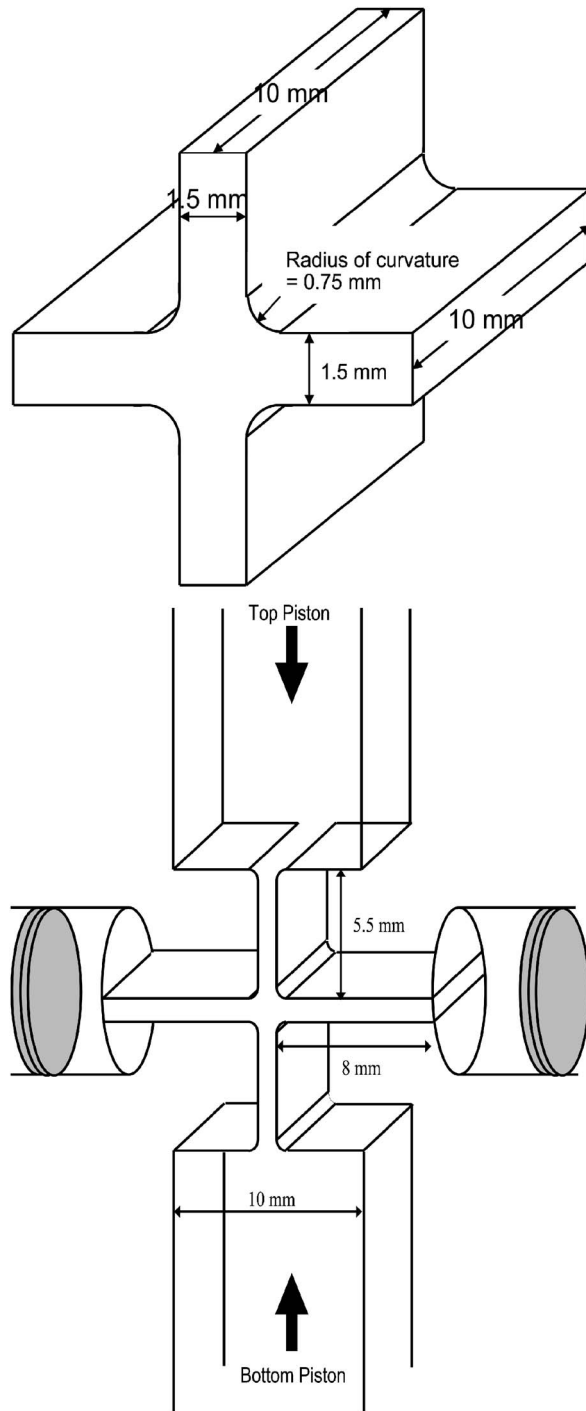
FIG. 2. Dimensions of cross-slot test section.

B. Materials

All of the polymer samples used in this paper were polyethylene. The polymers have been sourced from Dow Chemicals and Basell Polyolefins and are summarized in Table

FIG. 3. Cross-slot inserts.

I. A more detailed rheological characterization of the polymers is given in Appendix A. In order to obtain quantitative results from optical birefringence experiments, a value for the SOC has been determined for these polymers using optical long slit experiments within a multipass rheometer [see Coventry (2006)].

C. Characterization

A detailed characterization of the polymers' behavior in simple shear has been carried out using an Advanced Rheometric Expansion System (ARES) parallel plate rheometer. The method used followed the procedure described by Mackley *et al.* (1994) and consists of an oscillatory strain sweep to determine the range in which the polymers exhibit a linear response followed by a frequency sweep from which a spectrum of relaxation times was determined—the technique used for fitting relaxation modes follows that of Mead [see Mead (1994); Garcia-Franco and Mead (1999)]. The basic linear viscoelastic data are presented as an Appendix. Figures 10–12 show the rheological characterizations of PE CM3, LLDPE NG5056E, and LDPE 1800S, respectively. The results of the relaxation spectra have been expressed by plotting the product of the relaxation modulus and the relaxation time against the relaxation time. This shows the contribution of each of the modes to the zero-shear viscosity and clearly demonstrates the dominant relaxation modes. Finally a rate sweep experiment was done to measure the apparent viscosity at different rates of steady shear. The data show that, while some of the polymers follow the Cox–Merz rule [Cox and Merz (1958)] with reasonable accuracy for some of the range, deviations from this rule were also observed, particularly in the cases of the LDPE and LLDPE. Others [see, for example, White and Yamane (1987); Kalika and Denn (1987)] have noted that the Cox–Merz rule does not necessarily apply to all polyethylenes.

TABLE I. Polymers studied. Molecular weight averages and stress optical coefficient at 160 °C.

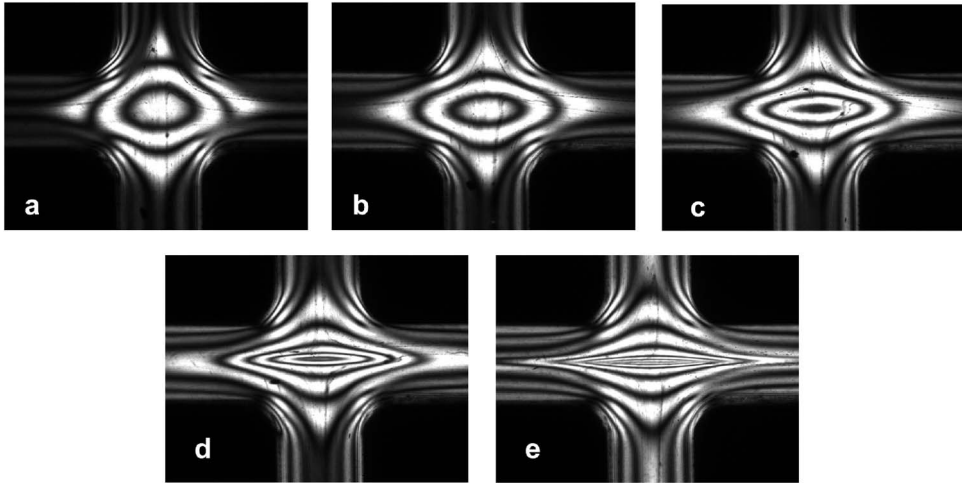| Designation	Type	M_w (g/mol)	Polydispersity (M_w/M_n)	SOC (m^2/N)
Dow CM3	Branched PE	84,000	2.20	2.1×10^{-9}
Dow NG5056E	LLDPE	113,000	2.20	1.8×10^{-9}
Basell 1800S	LDPE	107,000	15	2.2×10^{-9}

FIG. 4. Time dependent start-up flow for PE CM3 at a maximum extension rate of 1.5 s^{-1} and 155 °C. The images show the flow at (a) 0.5 s, (b) 1.0 s, (c) 1.5 s, (d) 2.2 s, and (e) 6.7 s after start-up.

III. RESULTS

A. Presentation of results

Experimental results are presented as optical birefringence from which a map of the principal stress difference can be generated from the experimentally determined stress optic coefficients. The data obtained from optical birefringence can therefore be presented either as an image or graphically. The image form presents a map of the principal stress difference at every point in the picture. Some results are presented in graphical form where the principal stress difference is followed along the inlet and exit symmetry plane (that is, the graphs represent line scans through the fringe photos along the inlet and outlet symmetry axes as shown in the insets in Figs. 5, 7, and 9). The zero order fringe line was determined from observation of the transient images. In this way both the buildup and relaxation of stress can be followed. For a purely Newtonian fluid these would be expected to be the same, however for viscoelastic fluids the inlet and outlet behavior will differ. Results presented in the center-line form are shown in Figs. 5, 7, and 9.

B. Start-up flow of a branched polyethylene

The sequence of images shown in Figs. 4(a)–4(e) show a time dependent start-up flow for the long chain branched polyethylene, CM3, at a temperature of 155 °C. A piston speed was chosen that gave a center-line extension rate of 1.6 s^{-1}. Initially (at time <0) the pistons were stationary and the polymer was fully relaxed. At $t=0$, both pistons were started and then moved at a constant velocity and the images represent the development in stress from the relaxed state at time=0, to a steady state flow pattern shown in Fig. 4(e).

A number of features are shown from these time dependent flow images. Both the magnitude of the stress and the degree of asymmetry between the inlet and outlet build with time until a steady state is reached. The stress pattern starts from a Newtonian form [Fig. 4(a)] where the center region inlet stress and outlet pattern is essentially symmetric.
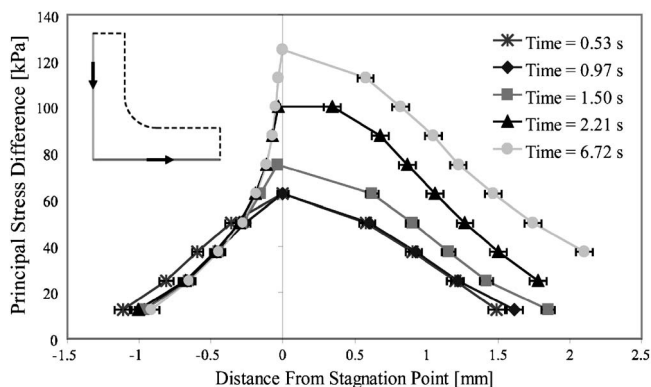
FIG. 5. Quantitative development of stress for PE CM3 start-up flow at 1.5 s^{-1} and 155 °C.

This shows that at early times the starting solution is Newtonian in form and at this early stage, the long relaxation modes within the polymer have had inadequate time to influence the stress field.

As time progresses the fringe/stress levels increase and the shape of the central region stress pattern changes [Figs. 4(b) and 4(c)]. The initially circular profile fringes become elliptical with the major axis of the ellipse oriented along the exit symmetry plane. This is an indication of mild viscoelasticity within the central region, where chain orientation develops as a consequence of the extensional strain and strain rate in the central stagnation point region of the flow. With a further development of time [Figs. 4(d) and 4(e)], the stress pattern develops a center-line cusping as the anisotropy near the exit plane of the stress pattern becomes progressively more anisotropic. Between Figs. 4(d) and 4(e) the fringes have evolved to give center-line cusps in the region of the exit symmetry plane. This shows that stress levels are highest very close to the exit symmetry plane and there is a high level of anisotropy between the inlet and outlet symmetry plane.

The development of steady state center-line stress buildup and relaxation is shown graphically in Fig. 5. Here the inlet and outlet principal stress differences are plotted for different times. At early times the inlet and outlet stress profile is similar, however as time evolves the stress patterns become very different reflecting the effect of strain history in different regions of the flow. Stress levels increase at the central stagnation point and relaxation of the stress extends along the exit symmetry plane of the geometry.

The photographs shown in Fig. 4 also allow comparison of stress levels between simple shearing flow that occurs near the inlet and outlet wall with the extensional stresses of the pure shear central region. It can be seen that the fringe number near the wall is very much lower than the central region fringe number indicating that extensional stresses are higher than shear stresses for this particular flow problem. In addition, the time dependence for stress buildup in the simple shear and extensional stress regions is different. Steady state in the simple shear region near the wall has essentially been reached by Fig. 4(c), whereas the extensional stress is still evolving. This is a clear indication that the long relaxation modes within the polymer play a greater role in the extensional flow.
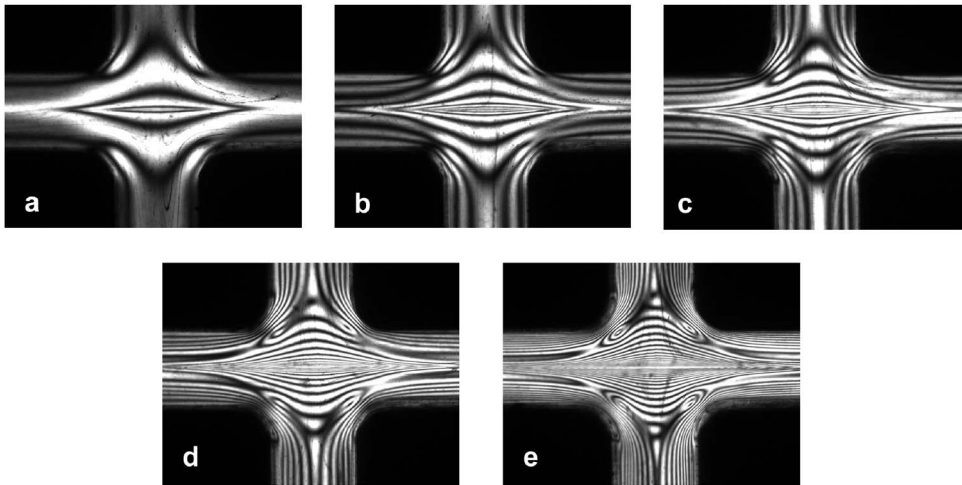
FIG. 6. Steady state stress fields with increasing extension rate for PE CM3 at 155 °C and (a) 0.6 s^{-1}, (b) 1.5 s^{-1}, (c) 3.1 s^{-1}, (d) 6.2 s^{-1}, and (e) 12.3 s^{-1}.

C. Comparison of steady-state stress fields at different extension rates

The effect of different piston speeds (center-line extension rate) is shown in Fig. 6 for the CM3 polyethylene at a temperature of 155 °C. The photographs correspond to the steady state values of the fringe patterns obtained when the MPR pistons had moved from rest for a sufficiently long time in order that the fringe patterns did not change with time. At all flow rates shown in Figs. 6(a)–6(e) center-line cusping was observed for the steady state condition. Figure 6(a) shows two highly cusped fringes in the central region. With increasing piston speed, the number of fringes increases although the form of the fringe pattern remains similar. Beyond Fig. 6(d), because of the increased number of fringes it becomes difficult to resolve the number of fringes that are present, although in principle these can be determined by following the fringe count on the cessation of flow. For this polymer the flows were observed to be stable at all flowrates tested and a picture emerges of development of stress both in the central region and at the walls of the cross slot.

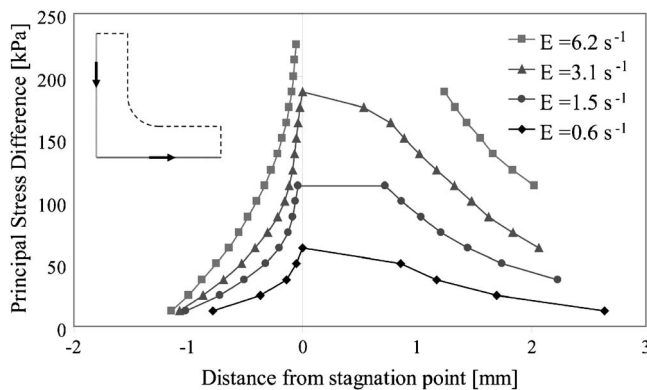The quantitative center-line development and relaxation of stress is shown in Fig. 7.

FIG. 7. Quantitative representation of steady state stress fields with increasing extension rate for PE CM3 at 155 °C. At high extension rates it is difficult to exactly measure the highest values for stress.
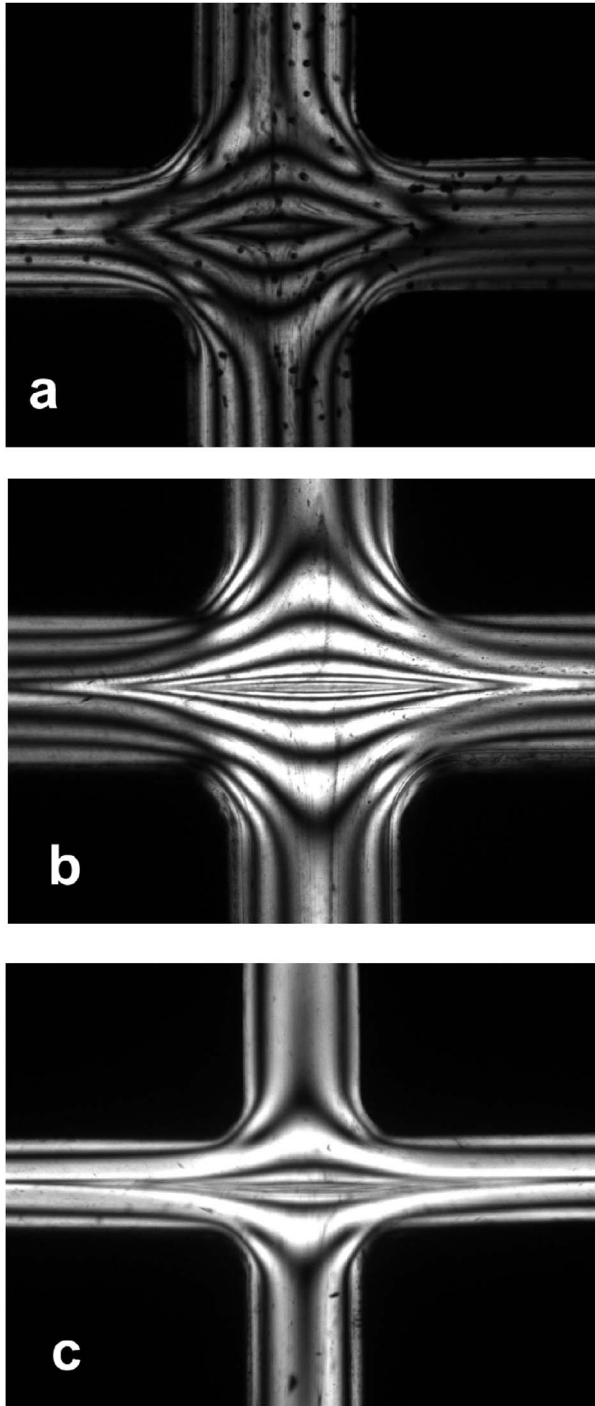
FIG. 8. Stress images for three different polymers. (a) LLDPE NG5056E at 3.1 s^{-1} and 160 °C. (b) PE CM3 at 1.5 s^{-1} and 155 °C. (c) LDPE 1800S at 12.3 s^{-1} and 160 °C.
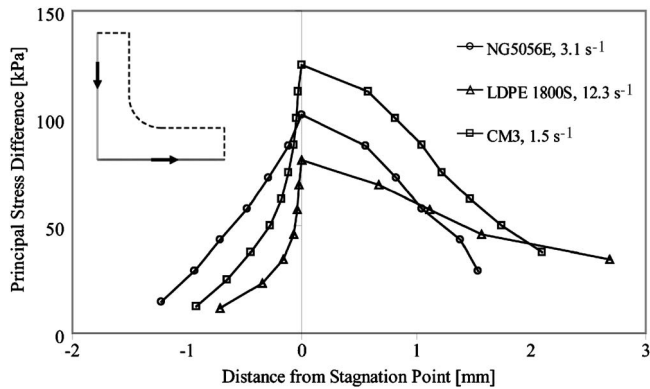
FIG. 9. Quantitative representation of rates of stress buildup and relaxation for different polymers.

Because of the high concentration of fringes at high flowrates along the exit symmetry plane it was not possible to capture the full stress profile for the highest piston speed. The data show the high level of anisotropy between the inlet and outlet of the flow at all flowrates and also the influence of the long relaxation modes on the development and relaxation of extensional stresses. It should be noted that the maximum value of birefringence and corresponding stress is well below that expected for full chain extension and this indicates that the origin of the birefringence is dominantly entropic orientation stress and not chain stretch.

D. Comparison of viscosity of steady-state stress fields for different polymers

The effect of different polymer viscoelasticity in cross-slot flow is qualitatively illustrated for three different polymers in Fig. 8. All of the polymers are polyethylenes; one LLDPE has short chain branching, another PE CM3 has limited long chain branching and finally one LDPE has extensive branching. Unfortunately, quantitative branching data were not available for each polymer; however, the relative level of viscoelasticity can be seen from the relaxation spectra given in the Appendix. The flow conditions are not exactly the same in terms of both temperature and flowrate, however the differences in the flow patterns are representative of the polymer type in the flow regimes shown. The respective rheology of each polymer is given in the Appendix to this paper and from this it can be seen that both the zero shear viscosity and also the relaxation spectra are different for each polymer. The least branched LLDPE shown in Fig. 8(a) shows the least level of center-line stress concentration and cusping. In addition the center-line stress levels as indicated by fringe number are not significantly greater than the wall fringe number. As branching increases [Figs. 8(b) and 8(c)] the degree of center-line stress localization increases. In Fig. 8(b) the stress level along the exit symmetry plane is many times that at the wall of the cross-slot. The magnitude of localization in Fig. 8(c) is difficult to fully quantify, however it is clear that with increasing branching there is increased localization of the center-plane stress field. The center-line stress field contours are plotted in Fig. 9 and again show the development of anisotropy with branching.

From observations that we have made for different polymers at different flowrates it is clear that the cross-slot geometry is capable of detecting extensional rheology differences in different polymers that are not apparent from simple shear rheology or simple shear optical effects within channels. In particular, the degree of localization observed along the exit symmetry plane of the cross-slot appears to be particularly sensitive to the long relaxation modes that may exist within a polymer sample.

IV. CONCLUSIONS

This paper has shown that it is possible to modify an MPR rheometer to give precise cross-slot flow birefringence data using sample quantities as small as 10 g. The proof of concept examples shown in this paper were for essentially commercial polydisperse polymers, however because of the small quantities involved, monodisperse polymers can also be used. Our observations show that at start up, all flows evolve from an initial Newtonian solution and then center-line anisotropy develops with increasing flow and viscoelasticity. The level of anisotropy is a sensitive marker to the level of viscoelasticity in the flow and in any one photograph a full range of strain history is explored for essentially one particular pure shear extensional flowrate that can be controlled by piston speed.

The choice of geometry dimensions inevitably leads to a compromise in relation to the extent of two-dimensional flow within the cross-slot configuration. Dimensions have been chosen that give adequate fringe counts together with a belief that the presence of the optical windows is not significantly influencing the observed fringe pattern.

The experimental data show that extensional stress increases as expected with increasing flowrate for all polymers and that center-line viscoelastic relaxation can be quantified easily along the exit symmetry plane. Increasing branching in particular leads to increasing extensional stress, more localized fringes and longer center-line relaxation times.

The data provide benchmark studies from which numerical simulation can be carried out. Ideally the simulation should be three dimensional but from our own preliminary findings it appears that two-dimensional simulation can give satisfactory prediction.

APPENDIX

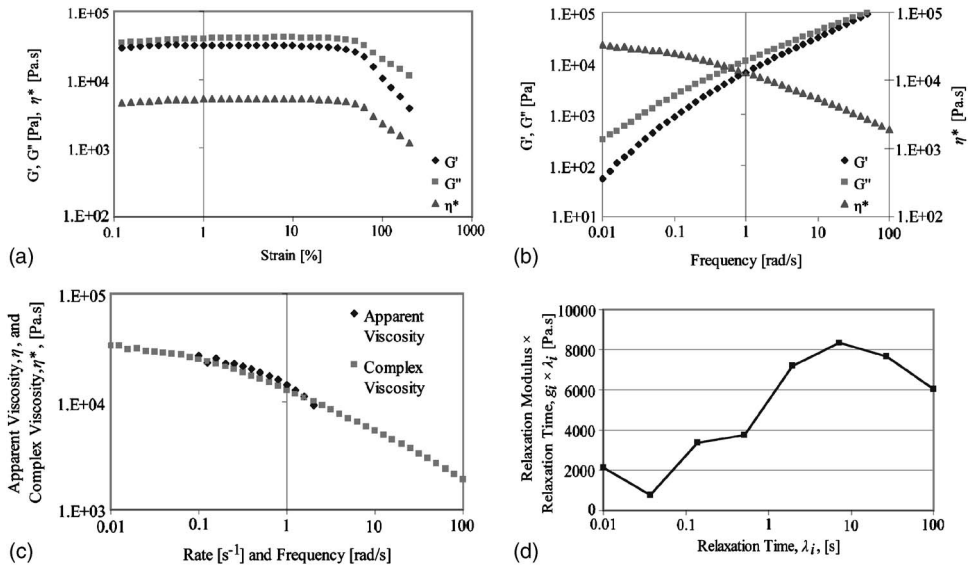See Figs. 10–12 for the basic linear viscoelastic data.

FIG. 10. Rheology of branched polyethylene CM3. (a) Strain sweep, $\omega = 10$ rad/s, (b) frequency sweep γ =10%, (c) comparison of steady shear apparent viscosity with complex viscosity, (d) spectrum of relaxation times.

FIG. 11. Rheology of LLDPE NG5056E. (a) Strain sweep, $\omega = 10$ rad/s, (b) frequency sweep $\gamma = 10\%$, (c) comparison of steady shear apparent viscosity with complex viscosity, (d) spectrum of relaxation times.
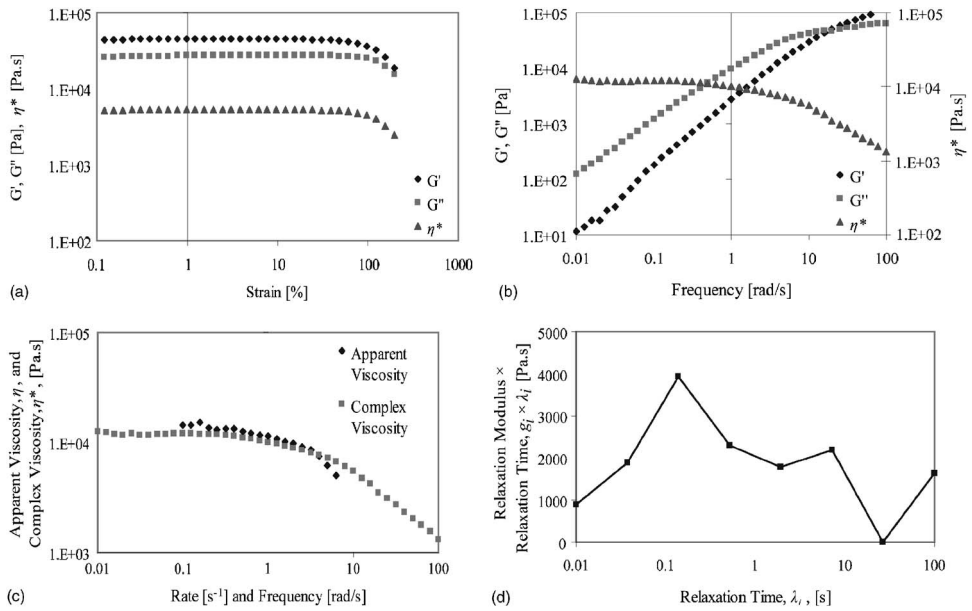
FIG. 12. Rheology of LDPE 1800S. (a) Strain sweep, $\omega = 10 \text{ rad/s}$, (b) frequency sweep $\gamma = 10\%$, (c) comparison of steady shear apparent viscosity with complex viscosity, (d) spectrum of relaxation times.
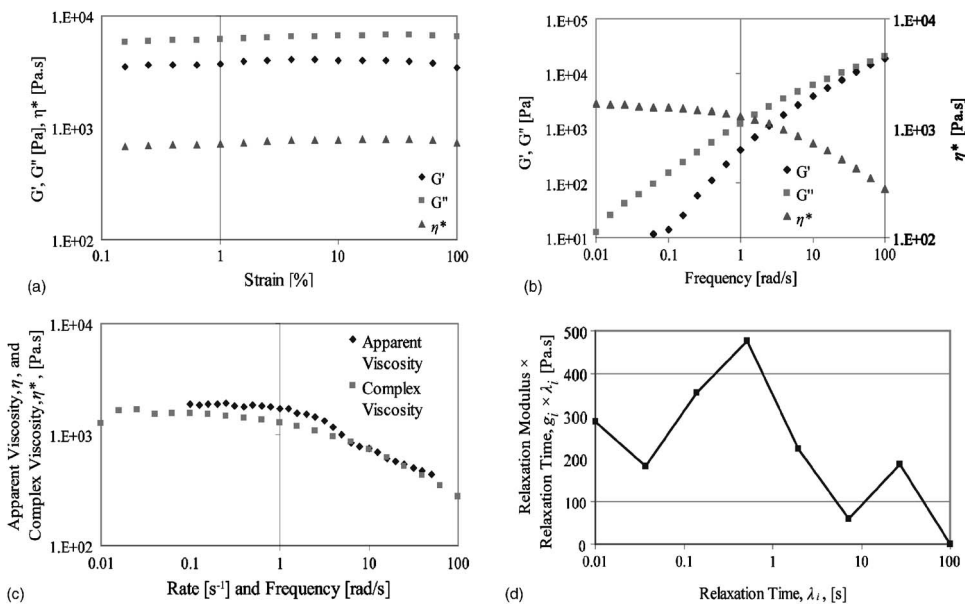
References

Clemeur, N., R. P. G. Rutgers, and B. Debbaut, "Numerical evaluation of three-dimensional effects in planar flow birefringence," J. Non-Newtonian Fluid Mech. **123**, 105–120 (2004).

Collis, M. W., and M. R. Mackley, "The melt processing of monodisperse and polydisperse polystyrene melts within a slit entry and exit flow," J. Non-Newtonian Fluid Mech. **128**, 29–41 (2005).

Coventry, K. D., "Cross-slot rheology of polymers," Ph.D. thesis, Department of Chemical Engineering, University of Cambridge (2006).

Cox, W. P., and E. H. Merz, "Correlation of dynamic and steady flow viscosities," J. Polym. Sci. **28**, 619–622 (1958).

Crowley, D. G., F. C. Frank, M. R. Mackley, and R. G. Stephenson, "Localized flow birefringence of polyethylene oxide solutions in a four roll mill," J. Polym. Sci. A **14**(2), 1111–1119 (1976).

Fuller, G. G., *Optical Rheometry of Complex Fluids* (Oxford University Press, New York, 1995).

Garcia-Franco, C. A., and D. W. Mead, "Rheological and molecular characterization of linear backbone flexible polymers with the Cole-Cole model relaxation spectrum," Rheol. Acta **38**, 34–47 (1999).

Kalika, D. S., and M. M. Denn, "Wall slip and extrudate distortion in linear low-density polyethylene," J. Rheol. **31**(8), 815–834 (1987).

Lee, K., M. R. Mackley, T. C. B. McLeish, T. M. Nicholson, and O. G. Harlen, "Experimental observation and numerical simulation of transient "stress fangs" within flowing molten polyethylene," J. Rheol. **45**(6), 1261–1277 (2001).

Mackley, M. R., R. T. J. Marshall, and J. B. A. F. Smeulders, "The multipass rheometer," J. Rheol. **39**(6), 1293–1309 (1995).

Mackley, M. R. R. T. J. Marshall, J. B. A. F. Smeulders, and F. D. Zhao, "The rheological characterization of polymeric and colloidal fluids," Chem. Eng. Sci. **49**(16), 2551–2565 (1994).

Mead, D. W., "Numerical interconversion of linear viscoelastic material functions," J. Rheol. **38**(6), 1769–1795 (1994).

Meissner, J., T. Raible, and S. E. Stephenson, "Rotary clamp in uniaxial and biaxial extensional rheometry of polymer melts," J. Rheol. **25**(1)1–28 (1981).

Miles, M. J., and A. Keller, "Conformational relaxation time in polymer solutions by elongational flow experiments: 2. Preliminaries of further developments: Chain retraction; identification of molecular weight fractions in a mixture," Polymer **21**, 1295–1298 (1980).

Munstedt, H., "New universal extensional rheometer for polymer melts. Measurements on a polystyrene sample," J. Rheol. **23**(4), 421–436 (1979).

Odell, J. A., and S. P. Carrington, "Extensional flow oscillatory rheometry," J. Non-Newtonian Fluid Mech. **137**, 110–120 (2006).

Pathak, J. A., and Hudson, S. D., "Rheo-optics of equilibrium polymer solutions: Wormlike micelles in elongational flow in a microfluidic cross-slot," Macromolecules **39**, 8782–8792 (2006).

Schoonen, J. F. M., "Determination of rheological constitutive equations using complex flows," Ph.D. thesis, Eindhoven University of Technology (1998).

Scrivener, O., C. Berner, R. Cressely, R. Hocquart, R. Sellin, and N. S. Vlaches, "Dynamical behaviour of drag-reducing polymer solutions," J. Non-Newtonian Fluid Mech. **5**, 475–495 (1979).

Sentmanat, M., B. N. Wang, and G. H. McKinley, "Measuring the transient extensional rheology of polyethylene melts using the SER universal testing platform," J. Rheol. **49**(3), 585–606 (2005).

Soulages, J., T. Schweizer, D. C. Venerus, J. Hostettler, F. Mettler, M. Kröger, and H. C. Öttinger, "Lubricated optical rheometer for the study of two-dimensional complex flows of polymer melts," J. Non-Newtonian Fluid Mech. **150**, 43–55 (2008).

Sridhar, T., V. Tirtaatmadja, D. A. Nguyen, and R. K. Gupta, "Measurement of extensional viscosity of polymer solutions," J. Non-Newtonian Fluid Mech. **40**, 271–280 (1991).

Taylor, G. I., "The formation of emulsions in definable fields of flow," Proc. R. Soc. London, Ser. A **A146**, 501–523 (1934).

Venerus, D. C., S.-H. Zhu, and H. C. Ottinger, "Stress and birefringence measurements during the uniaxial elongation of polystyrene melts," J. Rheol. **43**(3), 795–813 (1999).

Verbeeten, W. M. H., "Computational polymer melt rheology," Ph.D. thesis, Technische Universiteit Eindhoven (2001).

Verbeeten, W. M. H., G. W. M. Peters, and F. P. T. Baaijens, "Viscoelastic analysis of complex polymer melt flows using the eXtended Pom-Pom model," J. Non-Newtonian Fluid Mech. **108**, 301–326 (2002).

Wales, J. L. S., "The application of flow birefringence to rheological studies of polymer melts," Ph.D. thesis, Delft University (1976).

White, J. L., and H. Yamane, "A collaborative study of the stability of extrusion, melt spinning and tubular film extrusion of some high, low, and linear-low density polyethylene samples," Pure Appl. Chem. **59**, 193–216 (1987).